Structural Difference in Superconductive and Non-superconductive Bi–S Planes within $Bi_4O_4Bi_2S_4$ Blocks

Akira Miura[1*], Yoshikazu Mizuguchi[2*], Tsuyoshi Sugawara[2], Yongming Wang[3], Takahiro Takei[4], Nobuhiro Kumada[4], Eisuke Magome[5], Chikako Moriyoshi[5], Yoshihiro Kuroiwa[5], Osuke Miura[2], Kiyoharu Tadanaga[1]

1) Faculty of Engineering Hokkaido University, Kita 13, Nishi 8, Sapporo 060-8628 Japan, 2) Department of Electrical and Electronic Engineering, Tokyo Metropolitan University, 1-1 Minami-osawa, Hachioji, Tokyo 192-0397 Japan, 3) Creative Research Institution Hokkaido University, Kita 21, Nishi1 0, Sapporo 001-0021, Japan, 4) Center for Crystal Science and Technology, University of Yamanashi, 7-32 Miyamae, Kofu 400-8511 Japan, 5) Department of Physical Science, Hiroshima University, 1-3-1 Kagamiyama, Higashihiroshima, Hiroshima 739-8526 Japan.

Supporting Information Placeholder

ABSTRACT: The relationship between the structure and superconductivity of $Bi_4O_4S_3$ powders synthesized by heating under ambient and high pressures was investigated using synchrotron X-ray diffraction, Raman spectroscopy and TEM observation. The $Bi_4O_4S_3$ powders synthesized under ambient pressure exhibited a strong superconductivity (diamagnetic) signal and zero resistivity below ~4.5 K, while the $Bi_4O_4S_3$ powder synthesized by the high-pressure method exhibited a low intensity signal down to 2 K. Further annealing of the latter $Bi_4O_4S_3$ powder under ambient pressure led to the development of a strong signal and zero resistivity. The crystal structures of all $Bi_4O_4S_3$ phases consisted of $Bi_4O_4Bi_2S_4$ blocks including Bi–S layer and anion(s) sandwiched between $Bi_4O_4Bi_2S_4$ blocks, but minor structural differences were detected. Comparison of the structure of the superconductive and non-superconductive $Bi_4O_4S_3$ samples suggested that the superconductive $Bi_4O_4S_3$ phases had slightly smaller lattice parameters. The average structures of the superconductive $Bi_4O_4S_3$ phases were characterized by a slightly shorter and less bent Bi–S plane. Raman spectrum detected vibration of S–O bonds, which can be attributed to sandwiched anion(s) such as SO_4^{2-}. TEM observation showed stacking faults in the superconductive $Bi_4O_4S_3$ phases, which indicated local fluctuation of the average structures. The observed superconductivity of $Bi_4O_4S_3$ was discussed based on impurity phases, enhanced hybridization of the p_x and p_y orbitals of the Bi–S plane within $Bi_4O_4Bi_2S_4$ blocks, local fluctuation of the average structures, compositional deviation related to suspicious anion(s) sandwiched between $Bi_4O_4Bi_2S_4$ blocks, and the possibility of the suppression of the charge-density-wave state by enriched carrier concentrations.

Introduction

Superconductive materials are widely used in various areas such as medical diagnostics and energy transport. Superconductors require a large energy input for cooling to temperatures below the transition temperature. Thus, the development of new superconductors and understanding their mechanism of operation have remained challenging issues since the discovery of superconductivity. In 1986, copper-based layered oxides were found to be superconductors,[1] and in 2008, iron-based layered pnictides were discovered as superconductors.[2] In 2012, $Bi_4O_4S_3$ was reported as a new layered superconductor with $T_c \sim 5$ K.[3] Thereafter, a number of structurally-related layered BiS_2 superconductors were reported, such as $Bi_2(O,F)S_2$,[4] $Ln(O,F)BiS_2$,[5] $(Sr,Ln)FBiS_2$,[6] $Ln(O,F)BiSe_2$,[7] and $Eu_3Bi_2S_4F_4$.[8] These BiS_2 compounds have been recognized as a new class of layered BiS_2 superconductors[9] with T_c values of up to ~10 K.[10] The compositional and structural diversity demonstrates the potential to further increase the transition temperature of BiS_2 superconductors and also provides a key for understanding the mechanism underlying superconductivity.

$Bi_4O_4S_3$ is the first-discovered BiS_2 superconductor, and its superconductivity is considered to be related to the hybridized p_x and p_y orbitals between Bi and S.[3] $Bi_4O_4S_3$ can also be described as $Bi_4O_4Bi_2S_4(SO_4)_{1-x}$ (x = 0.5), in which sulfate anions are sandwiched by $Bi_4O_4Bi_2S_4$ blocks (Fig. 1). Different groups confirmed the superconductivity of this material via transport,[3, 11] magnetic[3, 11], specific heat[12], and muon-spin-spectroscopy measurements[13]. However, the impurities and structure of $Bi_4O_4S_3$ remain controversial. The reported X-ray diffraction patterns of $Bi_4O_4S_3$ powder samples invariably show impurity peaks, and single crystals of $Bi_4O_4S_3$ have not been successfully synthesized. Similar compounds, such as $Bi_3O_2S_3$[14] and Bi_2OS_2,[4] were recently reported; these are possibly coexisting impurity phases of $Bi_4O_4S_3$. Phelan et al. suggested that the stacking faults of $Bi_4O_4S_3$ could lead to more complicated compounds: $Bi_4O_4Bi_2S_4(S_2)_{1-x}(S)_x$.[14] Sathish et al. characterized $Bi_4O_4S_3$ samples synthesized through ambient-pressure and high-pressure methods by analysis of the X-Ray diffraction, magnetic, and transport properties.[15] They reported that the superconductivity of $Bi_4O_4S_3$ samples was plausibly attributed to an impurity phase(s), though they found minor structural difference between the $Bi_4O_4S_3$ phases synthesized under ambient and high pressure. Thus, the question of which crystal structures or impurities induce the superconductivity of $Bi_4O_4S_3$ samples remains open. Although structural analysis based on laboratory XRD have been performed, synchrotron X-ray diffraction is a powerful tool for

addressing this question since this technique can detect small amounts of impurity phase(s) and provides more reliable structural information. Further, TEM observation furnishes information about the local structure, such as stacking faults in layered structures, and Raman spectroscopy revealed the information of sandwiched anion(s).

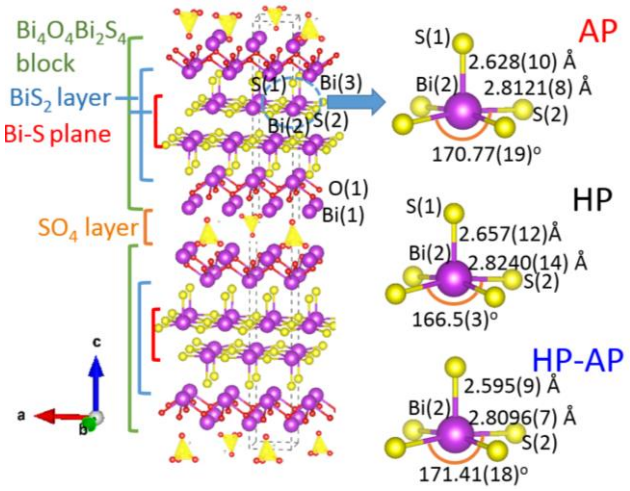

FIFURE 1. Crystal structure of $Bi_4O_4S_3$. Right schemes are structures of BiS_2 layers in $Bi_4O_4S_3$; AP: synthesized in a quartz tube at 510 °C; HP: at 700 °C/3 GPa, and HP-AP: with subsequent annealing at 510 °C. Unit cell is marked by dotted lines.

In this paper, we examine the structures and impurities in $Bi_4O_4S_3$ samples synthesized via ambient- and high-pressure methods in order to reveal the correlation between crystal structure and superconductive properties of the first-discovered BiS_2 superconductor. Synchrotron X-ray diffraction, TEM and Raman analyses provide detailed information about the structure and impurities of $Bi_4O_4S_3$, and reveal that minor structural changes in the Bi–S layer within $Bi_4O_4Bi_2S_4$ blocks are correlated to the superconductive properties.

Experimental

Three approaches were employed for synthesis of $Bi_4O_4S_3$ from Bi_2S_3, Bi_2O_3, and S powders using the stoichiometric ratio. The first synthesis was performed in an evacuated quartz tube under ambient pressure at 510 °C, as described in a previous report[3]; the sample thus-obtained is denoted AP $Bi_4O_4S_3$. The second was a high-pressure method using a cubic-anvil high-pressure apparatus with a 180 ton press operated at 700 °C/3 GPa for 1 h (sample HP $Bi_4O_4S_3$). The third method involved further annealing of HP $Bi_4O_4S_3$ in an evacuated quartz tube under ambient pressure at 510 °C (sample HP-AP $Bi_4O_4S_3$). Synchrotron X-ray powder diffraction measurements were performed at room temperature at the BL02B2 experimental station of SPring-8 (JASRI; Proposal Nos. 2014B1003, 2014B1071, and 2015A1441). The wavelength of the radiation beam was 0.49542(8) Å. Structural refinement was performed using RIETAN-FP[16] and Dysnomia,[17] and crystal structures were drawn with VESTA.[18] Vibration of the S-O bonds was evaluated via Raman microscopy. The local structure was examined via transmission electron microscopy (TEM). The temperature dependence of resistivity was measured by four-terminal method. The magnetic susceptibility was measured by using a superconducting quantum interference device (SQUID) magnetometer with a magnetic field of ~ 4.5 Oe after zero-field cooling.

Results

Figure 2 shows the synchrotron XRD profiles of the three $Bi_4O_4S_3$ powders: AP, HP, and HP-AP. Table 1 exhibits the summary of the analysis. For all samples, the main phases were indexed as tetragonal phases with long *c*-axes. The large lattice parameters were indicted by the peaks around 1.38° (d ~ 20.7 Å), which were indexed as the 002 peak of the tetragonal $Bi_4O_4S_3$ phase (Figure S1). The calculated mass fractions of the $Bi_4O_4S_3$ phase were 82.6, 89.6, and 93.1 % for AP, HP, and AP-HP $Bi_4O_4S_3$, respectively (Table 1). Bi and Bi_2S_3 impurities were also found. Approximately 3 mass% of the Bi_2OS_2 phase appeared only in $Bi_4O_4S_3$ (AP); a weak peak appeared at 2.06° (d ~ 13.8 Å) and was indexed as the 001 peak of the Bi_2OS_2 phase (Figure S1)[19]. The lattice parameters of the AP $Bi_4O_4S_3$ and HP-AP $Bi_4O_4S_3$ phases were slightly shorter than that found in HP $Bi_4O_4S_3$ (AP: a = 3.96398(5) Å, c = 41.2907(7) Å, HP: a = 3.96610(8) Å, c = 41.5046(11) Å, HP-AP: a = 3.96228(3) Å, c = 41.26192(4) Å).

Table 1. Summary of Rietveld refinements of AP $Bi_4O_4S_3$, HP $Bi_4O_4S_3$, and HP-AP $Bi_4O_4S_3$ powders

Samples	AP $Bi_4O_4S_3$				HP $Bi_4O_4S_3$			HP-AP $Bi_4O_4S_3$	
Number of phases	4				3			2	
Phase	$Bi_4O_4S_3$	Bi_2OS_2	Bi_2S_3	Bi	$Bi_4O_4S_3$	Bi_2S_3	Bi	$Bi_4O_4S_3$	Bi_2S_3
Mass fraction (%)	82.6	3.1	4.9	9.4	89.6	8.0	2.3	93.1	6.9
System	Tetra	Tetra	Ortho	Hex	Tetra	Ortho	Hex	Tetra	Ortho
Space Group	*I*4/*mmm*	*I*4/*mmm*	*Pnma*	*R*-3m	*I*4/*mmm*	*Pnma*	*R*-3*m*	*I*4/*mmm*	*Pnma*
Lattice parameter (a/Å)	3.96398(5)	3.96086	11.285	4.5412	3.96610(8)	11.322	4.546	3.96228(3)	11.281
Lattice parameter (b/Å)	3.96398(5)	3.96086	3.9756	4.5412	3.96610(8)	3.9921	4.546	3.96228 (3)	3.9756
Lattice parameter (c/Å)	41.2907(7)	13.8024	11.144	11.849	41.5046(11)	11.170	11.85	41.26192(4)	11.129
R_B(%)	1.54	1.61	1.25	1.58	1.73	1.93	1.70	2.66	5.58
R_F(%)	0.81	0.85	0.88	0.85	0.93	0.92	1.00	1.65	1.84
R_{WP} (%)	5.24				3.34			3.35	
R_P (%)	3.36				2.05			1.82	
S	3.51				2.17			2.17	

As mentioned, $Bi_4O_4S_3$ can be described as $Bi_4O_4Bi_2S_4$ blocks with sandwiched $(SO_4)_x$; the value of *x* is 0.5 for $Bi_4O_4S_3$. The Rietveld refinements for the $Bi_4O_4Bi_2S_4$ blocks were straightforward and robust. No or small amounts of vacancies were found in the $Bi_4O_4Bi_2S_4$ blocks for all samples; thus, further refinements were performed with full occupations. We focus on the coordination of Bi(2) and the S(2) plane, which is considered as a superconductivity plane.[3] The Bi(2)–S(2) bond found in AP and HP-AP is slightly shorter than that in HP (AP: 2.8121(8) Å, HP: 2.8240(10) Å, HP-AP: 2.8096(7) Å) and the S(2)–Bi(2)–S(2) angle in AP and HP-AP is less acute (AP: 170.77(19)°, HP: 166.5(3)°, HP-AP: 171.41(18)°). Though trials with different sandwiched species (SO_4^{2-}, S^{2-}, S_2^{2-}) affected the fitting parameters, the coordination of the Bi(2)–S(2) plane was not significantly changed (Table S5-6). Anion(s) sandwiched between $Bi_4O_4Bi_2S_4$ blocks were examined by Raman spectroscopy. The Raman shift at ~970 cm^{-1} was detected in the spectra of all three samples(Figure 3), which can be attributed to SO_4 tetrahedrons.[20] This Raman signal was stable during a few ten minutes, thus the laser-induced decomposition of the $Bi_4O_4S_3$ samples was unlikely. Nonetheless, these results cannot rule out the possible coexistence of other S-O/S^{2-}/S_2^{2-} species. Final refinements were performed by the assumption that SO_4 tetragonal with half occupancy was sandwiched between $Bi_4O_4Bi_2S_4$ blocks. Trials with freely-refined S and O suggested the existence of multiple positions along the 00*z* within the interlayered space. We proposed a model comprising upward as well as downward SO_4 tetrahedrons rotating along the *c*-axis (Figure 1), thereby achieving low refinement parameters (AP: R_{wp} = 5.24 %, HP: R_{wp} = 3.34 %, HP-AP: R_{wp} =3.35 %) with reasonable bonding distances around the SO_4 tetrahedron (Table S4) and electron density without remarkable ghost spots (Figure S2).

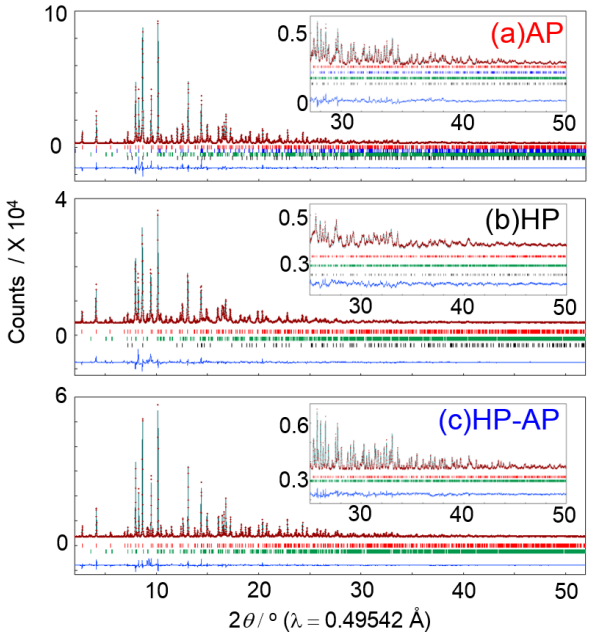

FIGURE 2 Rietveld profile of synchrotron X-ray diffraction of (a) AP $Bi_4O_4S_3$, (b) HP $Bi_4O_4S_3$, and (c) HP-AP $Bi_4O_4S_3$. Red dots and black lines indicate experimental and calculated points. Residuals are indicated by blue lines. Red, blue, green, and black bars show allowed diffractions of $Bi_4O_4S_3$, Bi_2OS_2, Bi_2S_3, and Bi, respectively.

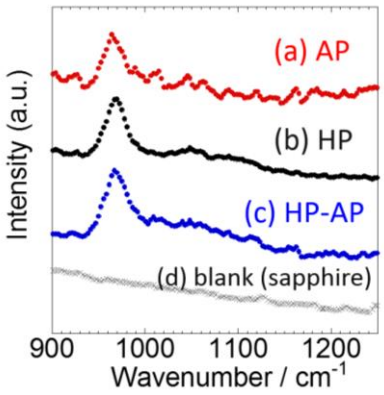

FIGURE 3 Raman spectra of (a) AP $Bi_4O_4S_3$, (b) HP $Bi_4O_4S_3$, (c) HP-AP $Bi_4O_4S_3$ and (d) sapphire substrate.

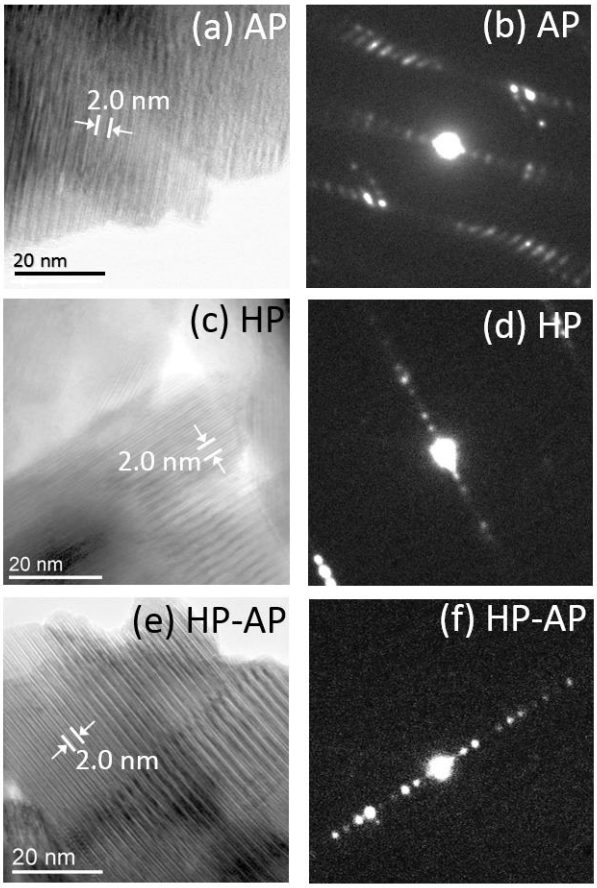

FIGURE 4 High-resolution TEM images (×300,000) and corresponding electron diffraction of (a, b) AP $Bi_4O_4S_3$, (c, d) HP $Bi_4O_4S_3$, and (e, f) HP-AP $Bi_4O_4S_3$.

Figure 4 presented typical high-resolution TEM images showing lattice fringes and corresponding electron diffraction; lower magnification images are shown in Fig. S3. The fringes of 2.0 nm corresponds to the approximate distance between the anion layers sandwiched between $Bi_4O_4Bi_2S_4$ blocks. The TEM and electron diffraction images of AP $Bi_4O_4S_3$ show significant amounts of stacking faults with diffused diffraction streaks along the c-axis (Fig. 4(a, b)). On the other hand, fewer stacking faults were observed for HP and HP-AP $Bi_4O_4S_3$ with relatively clear diffraction spots (Fig. 4 (c-f)).

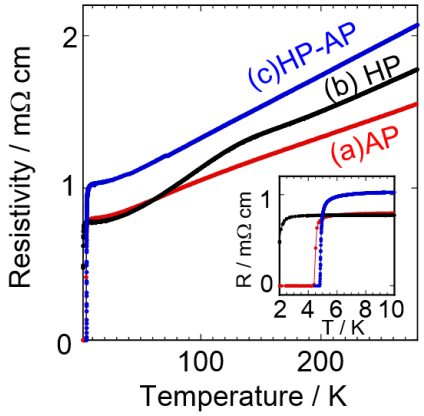

FIGURE 5 Temperature dependence of electronic resistivity down to 2 K of (a) AP $Bi_4O_4S_3$, (b) HP $Bi_4O_4S_3$, and (c) HP-AP $Bi_4O_4S_3$.

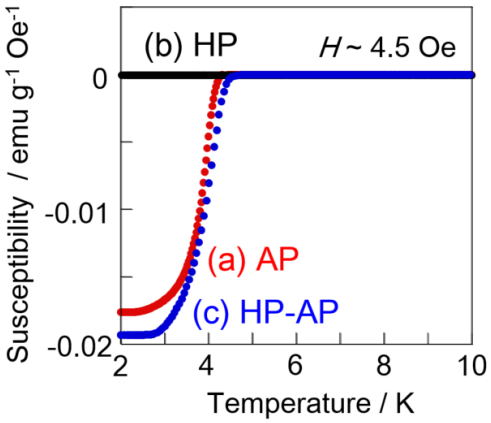

FIGURE 6 Temperature dependence of magnetization between 2-10 K of (a) AP $Bi_4O_4S_3$, (b) HP $Bi_4O_4S_3$, and (c) HP-AP $Bi_4O_4S_3$.

Heating under ambient pressure significantly affected the conductive and magnetic properties of $Bi_4O_4S_3$. Figure 5 shows the electronic resistivity of three $Bi_4O_4S_3$. All the samples exhibited metallic behavior in the normal region. AP $Bi_4O_4S_3$ showed zero resistivity at 4.4 K. Contrastingly, HP-$Bi_4O_4S_3$ displayed the possible onset of superconductive transition at ~ 2.3 K, but zero resistivity was not observed. The hump of resistivity at around 150 K was seen. Further annealed HP-AP $Bi_4O_4S_3$ exhibited zero resistivity. HP-AP $Bi_4O_4S_3$ showed zero resistivity at 4.8 K.

Figure 6 shows the magnetic properties of $Bi_4O_4S_3$. AP $Bi_4O_4S_3$ showed a strong diamagnetic signal (T_c~4.5 K). In contrast, HP-$Bi_4O_4S_3$ exhibited a low intensity diamagnetic signal. Further annealed HP-AP $Bi_4O_4S_3$ exhibited an intense diamagnetic signal. Thus, ambient pressure annealing is important for activating superconductivity.

Discussion

Zero resistivity of AP and HP-AP $Bi_4O_4S_3$ powders suggests that AP and HP-AP $Bi_4O_4S_3$ powders contain a superconductive phase. Large signals of magnetic susceptibility in AP and HP-AP $Bi_4O_4S_3$ powders can be attributed to either bulk superconductivity of $Bi_4O_4S_3$ phase or another superconductive phase

covering on non-superconductive particles. Specific heat jump of AP-$Bi_4O_4S_3$ sample has been reported at 4.4 K, which is an evidence of the bulk superconductivity of $Bi_4O_4S_3$ phase.[12] The relatively small specific heat jump, which has been also reported on many other BiS_2 superconductors[9], can be explained by a small electronic specific heat coefficient. However, it has been argued that this small specific heat jump can be attributed to a superconductive impurity.[15]

Synchrotron X-ray diffraction detected 82.6 and 93.1 % of $Bi_4O_4S_3$ phases in AP and HP-AP $Bi_4O_4S_3$ powders, respectively. AP $Bi_4O_4S_3$ powders showed Bi, Bi_2S_3 and Bi_2O_3 as impurities while HP-AP $Bi_4O_4S_3$ powder included Bi_2S_3 as an impurity. These impurities show no superconducting transition (Figure S4). Thus, comparable intensities with its volume fraction above unity of the diamagnetic signals found in AP and HP-AP $Bi_4O_4S_3$ can be attributed to superconductive $Bi_4O_4S_3$ phases. Superconductivity of Bi_2S_3, which is a common impurity in superconductive AP and HP-AP $Bi_4O_4S_3$ powders, is unlikely since it is also found in non-superconductive HP $Bi_4O_4S_3$ powder. Moreover, TEM observation showed clean surface layers on superconductive AP and HP-AP $Bi_4O_4S_3$ phases; no obvious impurity phases were observed on their surfaces. Therefore, our results of synchrotron X-ray diffraction and TEM observation support the bulk superconductivity of AP and HP-AP $Bi_4O_4S_3$ phases.

What is the crystallographic difference in superconductive and non-superconductive $Bi_4O_4S_3$ phases? Although impurity phases make difficult to derive accurate structural data by Rietveld analysis even using synchrotron X-ray radiation, their good fitting with impurity phases would ensure the atomic positions of $Bi_4O_4Bi_2S_4$ blocks above a fair degree of accuracy. Comparison of the crystal structures of $Bi_4O_4S_3$ shows that slightly shorter and less bent Bi(2)–S(2) bonds in $Bi_4O_4Bi_2S_4$ blocks occur in the superconductive AP and HP-AP $Bi_4O_4S_3$ phases. This suggests a correlation between enhanced overlap of the p_x and p_y orbitals of Bi(2) and S(2) and the superconductivity of the $Bi_4O_4S_3$ phases, similar to $Ln(O,F)BiS_2$ superconductors: Ln = La-Sm.[21] The observed stacking faults in all evaluated $Bi_4O_4S_3$ phases should produce local fluctuations of the average structures. However, the similarity of the superconductivity despite different amounts of stacking faults in AP and HP-AP $Bi_4O_4S_3$ suggests that more stacking faults (i.e. local fluctuations) do not significantly affect the superconductivity.

The exact compositions and structures of $Bi_4O_4S_3$ are still suspicious because of the anion(s) sandwiched by $Bi_4O_4Bi_2S_4$ blocks. Raman spectroscopy detected S-O vibrations in all the $Bi_4O_4S_3$ powders, thus SO_4^{2-} was a candidate as the anion. However, Raman spectroscopy did not deny the possible coexistence of other species S^{2-}, S_2^{2-} or other S-O species between $Bi_4O_4Bi_2S_4$ blocks. The shorter lattice parameters of superconductive AP- and HP-AP $Bi_4O_4S_3$ phases were detected, which could be attributed to less sandwiched atoms. Stacking faults can be caused by inhomogeneous anion(s) between $Bi_4O_4Bi_2S_4$ blocks. The pressure in the vacuum glass capillary increased after annealing HP $Bi_4O_4S_3$ powder, as confirmed by the inflated headspace of the capillary after heating using a burner. Thus, the compositional difference among $Bi_4O_4S_3$ phases are most likely, which can affect the lattice parameters, stacking faults, and superconductivity. Further investigation, such as neutron diffraction or single-crystal analysis, might clarify their exact chemical formula and lattice parameters as well as more precise structural information.

A possible explanation for the observed superconductivity is a change in a charge-density-wave state and carrier concentrations. Higher carrier concentrations are likely in the superconductive AP and HP-AP $Bi_4O_4S_3$ phases; this is indicated by the less-bent Bi(2)–S(2) plane according to a previous study of the relationship between the carrier concentration and Bi–S plane in $Ln(O,F)BiS_2$.[21a, 21b] A charge-density wave state was implicated by the electronic resistivity hump at around 150 K, observed only for non-superconductive HP $Bi_4O_4S_3$; this feature was not found in superconductive AP and HP-AP $Bi_4O_4S_3$. A similar hump was observed for $EuBiS_2F$,[6b] which was explained by a possible charge-density-wave transition. Thus, superconductivity can be induced by suppression of the charge-density-wave states, which may be related to enriched carrier concentrations.

Conclusion

Synchrotron X-ray diffraction analysis demonstrated the presence of more than 80 mass % of the superconductive $Bi_4O_4S_3$ phase consisting of $Bi_4O_4Bi_2S_4$ blocks and sandwiched anion(s). Heating in a vacuum tube was an important process for activating the superconductivity. Heating induced slight shrinkage of the lattice parameters and shorter and less bent Bi(2)–S(2) bond together with the appearance of superconductivity. Stacking faults in the superconductive phases did not significantly affect the superconductivity. Although Raman spectroscopy detected the vibration of S-O bonding, the correlation between the appearance of superconductivity and the species/amounts of sandwiched anion(s) remains as a further challenge. Suppression of the charge-density-state with enhanced carrier concentrations may explain the appearance of the superconductivity.

ASSOCIATED CONTENT

Supporting Information

Details of crystal structures and Raman spectra of $Bi_4O_4S_3$ are provided in Supporting Information.

AUTHOR INFORMATION

Corresponding Authors

A.M.: amiura@eng.hokudai.ac.jp, Y.M.: mizugu@tmu.ac.jp

Notes

The authors declare no competing financial interest.

Funding Sources

The experiments were partially supported by KAKENHI Grant Numbers 15K14113 and 25707031.

ACKNOWLEDGMENT

A.M. thanks Profs. T. Shimada, T. Nagahama, and T. Motohashi for help or suggestions for Raman spectroscopy and structural analyses. TEM observation was carried out at the "Joint-use Facilities: Laboratory of Nano-Micro Material Analysis", Hokkaido University.

REFERENCES

1. Bednorz, J. G.; Müller, K. A., Possible high Tc superconductivity in the Ba−La−Cu−O system. *Z. Phys. B Con. Mat.* **1986,** *64* (2), 189-193.

2. Kamihara, Y.; Watanabe, T.; Hirano, M.; Hosono, H., Iron-Based Layered Superconductor La(O1-xFx)FeAs (x = 0.05-0.12) with Tc = 26 K. *JACS* **2008,** *130* (11), 3296-3297.
3. Mizuguchi, Y.; Fujihisa, H.; Gotoh, Y.; Suzuki, K.; Usui, H.; Kuroki, K.; Demura, S.; Takano, Y.; Izawa, H.; Miura, O., BiS2-based layered superconductor Bi4O4S3. *Phy.s Rev. B* **2012,** *86* (22).
4. (a) Okada, T.; Ogino, H.; Shimoyama, J.-i.; Kishio, K., Topotactic synthesis of a new BiS2-based superconductor Bi2(O,F)S2. *APEX* **2015,** *8* (2), 023102; (b) Shao, J.; Yao, X.; Liu, Z.; Pi, L.; Tan, S.; Zhang, C.; Zhang, Y., Superconductivity in BiO1−xFxBiS2and possible parent phase of Bi4O4S3 superconductor. *Supercond. Sci. Technol.* **2015,** *28* (1), 015008.
5. (a) Mizuguchi, Y.; Demura, S.; Deguchi, K.; Takano, Y.; Fujihisa, H.; Gotoh, Y.; Izawa, H.; Miura, O., Superconductivity in Novel BiS2-Based Layered Superconductor LaO1-xFxBiS2. *J. Phys. Soc. Jpn.* **2012,** *81* (11), 114725; (b) Demura, S.; Mizuguchi, Y.; Deguchi, K.; Okazaki, H.; Hara, H.; Watanabe, T.; James Denholme, S.; Fujioka, M.; Ozaki, T.; Fujihisa, H.; Gotoh, Y.; Miura, O.; Yamaguchi, T.; Takeya, H.; Takano, Y., New Member of BiS2-Based Superconductor NdO1-xFxBiS2. *J. Phys. Soc. Jpn.* **2013,** *82* (3), 033708; (c) Jha, R.; Kumar, A.; Kumar Singh, S.; Awana, V. P. S., Synthesis and Superconductivity of New BiS2 Based Superconductor PrO0.5F0.5BiS2. *J. Supercond. Nov. Magn.* **2013,** *26* (3), 499-502.
6. (a) Lin, X.; Ni, X.; Chen, B.; Xu, X.; Yang, X.; Dai, J.; Li, Y.; Yang, X.; Luo, Y.; Tao, Q.; Cao, G.; Xu, Z., Superconductivity induced by La doping in Sr-xLaxFBiS2. *Phys. Rev. B* **2013,** *87* (2), 020504(R); (b) Zhai, H.-F.; Tang, Z.-T.; Jiang, H.; Xu, K.; Zhang, K.; Zhang, P.; Bao, J.-K.; Sun, Y.-L.; Jiao, W.-H.; Nowik, I.; Felner, I.; Li, Y.-K.; Xu, X.-F.; Tao, Q.; Feng, C.-M.; Xu, Z.-A.; Cao, G.-H., Possible charge-density wave, superconductivity, and f-electron valence instability in EuBiS2F. *Phys Rev B* **2014,** *90* (6); (c) Jha, R.; Tiwari, B.; Awana, V. P. S., Appearance of bulk superconductivity under hydrostatic pressure in Sr0.5RE0.5FBiS2 (RE = Ce, Nd, Pr, and Sm) compounds. *J. Appl. Phys.* **2015,** *117* (1), 013901.
7. (a) Krzton-Maziopa, A.; Guguchia, Z.; Pomjakushina, E.; Pomjakushin, V.; Khasanov, R.; Luetkens, H.; Biswas, P. K.; Amato, A.; Keller, H.; Conder, K., Superconductivity in a new layered bismuth oxyselenide: LaO(0.5)F(0.5)BiSe(2). *J. Phys Comdens Matter* **2014,** *26* (21), 215702; (b) Fujioka, M.; Tanaka, M.; Denholme, S. J.; Yamaki, T.; Takeya, H.; Yamaguchi, T.; Takano, Y., Pressure-induced phase transition for single-crystalline LaO0.5F0.5BiSe2. *Europhys. Lett.* **2014,** *108* (4), 47007; (c) Jha, R.; Awana, V. P. S., Anomalous Impact of Hydrostatic Pressure on Superconductivity of Polycrystalline LaO0.5F0.5BiSe2. *J. Supercond. Nov. Magn.* **2015,** *28* (8), 2229-2233.
8. Zhai, H. F.; Zhang, P.; Wu, S. Q.; He, C. Y.; Tang, Z. T.; Jiang, H.; Sun, Y. L.; Bao, J. K.; Nowik, I.; Felner, I.; Zeng, Y. W.; Li, Y. K.; Xu, X. F.; Tao, Q.; Xu, Z. A.; Cao, G. H., Anomalous Eu Valence State and Superconductivity in Undoped Eu3Bi2S4F4. *JACS* **2014**.
9. Yazici, D.; Jeon, I.; White, B. D.; Maple, M. B., Superconductivity in layered BiS2-based compounds. *Physica C Supercond* **2015,** *514*, 218-236.
10. Kotegawa, H.; Tomita, Y.; Tou, H.; Izawa, H.; Mizuguchi, Y.; Miura, O.; Demura, S.; Deguchi, K.; Takano, Y., Pressure Study of BiS2-Based Superconductors Bi4O43 and La(O,F)BiS2. *J. Phys. Soc. Jpn.* **2012,** *81* (10), 103702.
11. (a) Singh, S. K.; Kumar, A.; Gahtori, B.; Shruti; Sharma, G.; Patnaik, S.; Awana, V. P., Bulk superconductivity in bismuth oxysulfide Bi4O4S3. *JACS* **2012,** *134* (40), 16504-7; (b) Zhang, X.; Liu, Y.; Zhang, G.; Wang, Y.; Zhang, H.; Huang, F., Thermal Decomposition of Bismuth Oxysulfide from Photoelectric Bi2O2S to Superconducting Bi4O4S3. *ACS Appl Mater Inter* **2015**.
12. Takatsu, H.; Mizuguchi, Y.; Izawa, H.; Miura, O.; Kadowaki, H., Bulk Superconductivity in Bi4O4S3 Revealed by Specific Heat Measurement. *J. Phys. Soc. Jpn.* **2012,** *81* (12), 125002.
13. Biswas, P. K.; Amato, A.; Baines, C.; Khasanov, R.; Luetkens, H.; Lei, H.; Petrovic, C.; Morenzoni, E., Low superfluid density and possible multigap superconductivity in the BiS2-based layered superconductorBi4O4S3. *Phys. Rev. B* **2013,** *88* (22).
14. Phelan, W. A.; Wallace, D. C.; Arpino, K. E.; Neilson, J. R.; Livi, K. J.; Seabourne, C. R.; Scott, A. J.; McQueen, T. M., Stacking Variants and Superconductivity in the Bi–O–S System. *J. Am. Chem. Soc.* **2013,** *135* (14), 5372-5374.
15. I. Sathish, C.; Luke Feng, H.; Shi, Y.; Yamaura, K., Superconductivity in Bismuth Oxysulfide Bi4O4S3. *J. Phys. Soc. Jpn.* **2013,** *82* (7), 074703.
16. Izumi, F.; Momma, K., Three-dimensional visualization in powder diffraction. *Solid State Phenom.* **2007,** *130*, 15-20.
17. Izumi, F.; Momma, K., Three-dimensional visualization of electron- and nuclear-density distributions in inorganic materials by MEM-based technology. *IOP conf. ser., Mater. sci. eng.* **2011,** *18* (2), 022001.
18. Momma, K.; Izumi, F., VESTA: a three-dimensional visualization system for electronic and structural analysis. *J. Appl. Crystallogr.* **2008,** *41* (3), 653-658.
19. Akira Miura, Y. M., Takahiro Takei, Nobuhiro Kumada, Eisuke Magome, Chikako Moriyoshi, Yoshihiro Kuroiwa, Kiyoharu Tadanaga, Structures and Optical Properties of Bi2OS2 and LaOBiS2. *arXiv:1508.01635* **2015**.
20. Fadda, P., Effetto Raman degli ioniSO4 edSO3 e dissociazione elettrolitica degli acidi solforico e solforoso. *Nuovo Cim* **1932,** *9* (6), 168-179.
21. (a) Miura, A.; Nagao, M.; Takei, T.; Watauchi, S.; Mizuguchi, Y.; Takano, Y.; Tanaka, I.; Kumada, N., Structure, Superconductivity, and Magnetism of Ce(O,F)BiS2Single Crystals. *Cryst Growth Des* **2015,** *15* (1), 39-44; (b) Miura, A.; Nagao, M.; Takei, T.; Watauchi, S.; Tanaka, I.; Kumada, N., Crystal structures of LaO1−xFxBiS2 (x~0.23, 0.46): Effect of F doping on distortion of Bi–S plane. *J. Solid State Chem.* **2014,** *212*, 213-217; (c) Mizuguchi, Y.; Miura, A.; Kajitani, J.; Hiroi, T.; Miura, O.; Tadanaga, K.; Kumada, N.; Magome, E.; Moriyoshi, C.; Kuroiwa, Y., In-plane chemical pressure essential for superconductivity in BiCh2-based (Ch: S, Se) layered structure. *Sci Rep* **Accepted**.

Superconductive $Bi_4O_4S_3$ phases contain shorter and less bent Bi–S planes.